IEEE Robotics and Automation Letters (RA-L) paper, presented at ICRA 2026, Vienna, Austria. Cite as RA-L paper.

Sampling-aware Multi-rate Combined Control for an Orbital Manipulator

Ria Vijayan[1], Marco De Stefano[1], and Christian Ott[2]

***Abstract*—In on-orbit servicing missions using robotic manipulators, certain challenging scenarios require the use of combined control i.e. actuation of spacecraft and the manipulator, to meet mission requirements. The low frequency of the controller of the spacecraft compared to the manipulator can compromise the stability margin of the combined control. In this paper, we first design a combined control strategy to carefully decouple the high-rate manipulator control from the spacecraft's low-rate control. Second, we design a novel discrete controller accounting for the first-order effects of the servicer's low sampling rate. This is realized by augmenting a classical proportional-derivative (PD) control scheme. The operational bounds of the discrete controller are first benchmarked on a one-DoF system and further investigated for performance using a multi-DoF orbital manipulator. The results shed light on the regions of enhanced performance in terms of stability and impulse utilization as a measure of efficiency. Simulation results and hardware-in-the-loop experiments are performed to validate the proposed method.**

***Index Terms*—On orbit servicing, discrete control, multi-rate control, orbital robotic manipulator.**

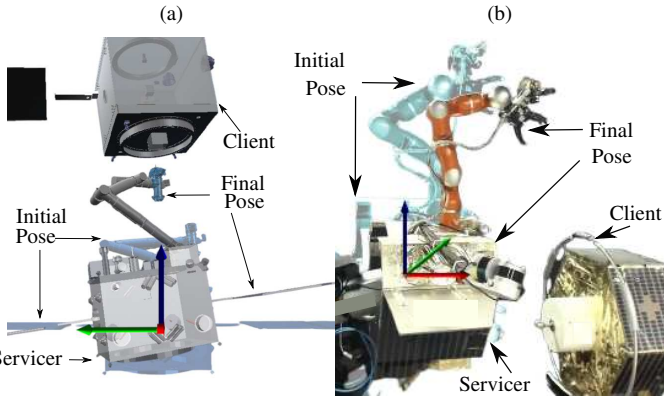

Fig. 1: Close-proximity maneuvers shown in (a) simulation and (b) with hardware-in-the-loop (DLR, OOS-Sim) using 7-DoF manipulators. The challenge in space missions is the combined control of the servicer, typically at low-rate, and the manipulator at high-rate. See accompanying video for experiments with the proposed method.

I. Introduction

In the context of on-orbit servicing (OOS), see Fig. 1, an orbital manipulator i.e. a *servicer* satellite equipped with a manipulator arm, plays a critical role in maintaining and servicing other spacecraft (clients). To meet different mission requirements, certain challenging scenarios in OOS (eg. synchronized approach to a drifting client) require active control of both the servicer and manipulator, called *combined control*, coordinated control or free-flying control in the literature.

The complexity of combined control is compounded by the fact that the servicer satellite and its manipulator arm are controlled at different frequencies. The spacecraft control typically operates at a relatively low frequency below 10Hz, while the manipulator arm, which requires precise movements, is controlled at a much higher rate of approximately 1kHz [1]. This disparity in control frequencies means that the servicer's control is discrete, whereas the manipulator's control is quasi-continuous. This is what we refer to as *multi-rate* control in the scope of this work for combined control of an orbital manipulator. If not carefully designed, the low sampling and actuation rate of the servicer satellite can cause instabilites due to energy leaks from the time-delays introduced by a sampled-data system [2] (demonstrated on hardware in [3]).

The design of sampled-data controllers is examined in [4] through Lyapunov function matching at the sampling instants to stabilize a backstepping controller. Stability of haptic rendering under effects of discretization, quantization, time delay, and coulomb effects are studied in [2] for the one degree-of-freedom (DoF) case. An approach with variable samplings has been proposed in [5] to stabilize a nonholonomic system linearized about its equilibrium. A feedback passivation controller is applied in discrete time for matching the energy consumption at all sampling instants along the closed-loop system [6]. A sampled-data control based on discrete-time equivalent model is proposed for a class of nonlinear time-delay systems in [7]. A variable rate digital feedback control algorithm using a series expansion is proposed to preserve the stability of the continuous-time controller at the sampling instants in [8]. A passivating and stabilizating controller is proposed in [9] for a discrete-time nonlinear systems via energy balancing by assigning a target energy profile at all sampling instants. A combination of discrete- and continuous-time elements is used in [10] to present passivity and stability analysis of a one DoF discrete system with time-delay.

Discrete-time controllers have also been studied in the context of spacecraft control. A guidance algorithm based on feedback linearization was designed while considering a modulation scheme with adaptation of the control gains for discrete-variable actuation in [11]. An adaptive robust control approach was implemented with the disturbance estimation used as feed-forward to attenuate the disturbance effects in [12]. A saturated feedback law for the propulsion was designed with quasi-global analytical stability properties for use in

Manuscript received: September 26 2025; Revised December 19 2025; Accepted December 30 2025. A video accompanies this manuscript.

[1]Ria Vijayan and Marco De Stefano are with the Institute of Robotics and Mechatronics, German Aerospace Center (DLR). Ria.Vijayan@dlr.de

[2]Christian Ott is with TU Wien and DLR.

IEEE Robotics and Automation Letters (RA-L) paper, presented at ICRA 2026, Vienna, Austria. Cite as RA-L paper.

nonlinear orbit control [13]. A discrete-time nonlinear attitude tracking controller resulting in semiglobal practical asymptotic stability was developed in [14] considering sampling effects of digital control. An adaptive sliding mode controller was shown to ensure uniformly ultimately bounded stability while considering actuator faults and disturbances in [15]. A discrete-time sliding mode control suppressing chattering was designed in [16] for the finite-time attitude tracking control problem of spacecrafts with flexible structures. A model predictive control with discontinuities and constraints was designed for the attitude dynamics of an underactuated spacecraft and shown to be asymptotically stable [17]. In [18] a model predictive controller was proposed to incorporate deadband constraints utilizing convex optimization techniques to handle the discrete nature of actuators in rendezvous missions. In contrast to [19] which dissipates active energy detected by a passivity observer, the proposed method acts a priori based on theoretical deduction to reduce system activity.

This paper focuses on the design and analysis of a multi-rate combined control of a multi-DoF system, while accounting for the coupling between subsystems controlled at different rates. This is done for an orbital manipulator that is considered to have low-rate (eg. 10Hz) actuation for the spacecraft base and high-rate (eg. 1kHz) actuation for the manipulator. The proposed method uses two key approaches. The first is a combined control strategy carefully designed to decouple the high-rate manipulator control from the spacecraft's discrete control. The second is the design of a discrete controller that compensates the first-order effects of the servicer's low sampling rate. This is realized by augmenting a classical PD control scheme using discrete Lyapunov analysis. The proposed controller is benchmarked on a one-DoF system before investigating its operational bounds for the multi-DoF orbital manipulator.

The contributions of this paper can be summarized as:

- A novel combined control strategy applied to an orbital manipulator operated under a multi-rate control scheme.
- A novel discrete PD control that accounts for first-order sampling effects.
- Validation and analysis in simulation of the performance of the proposed multi-rate combined controller.
- Validation of the proposed multi-rate combined controller using hardware-in-the-loop (HIL) experiments.

II. Multi-rate operation: Preliminaries and problem statement

In this section we recall the preliminaries on dynamics of an orbital manipulator and define the conditions and assumptions of its multi-rate operation. Finally, we define the problem statement considered for the scope of this work.

A. Dynamics of an orbital manipualtor

The nonlinear coupled dynamics of a spacecraft base with a manipulator with n joints can be written using the standard floating-base robot dynamics as

$$\begin{bmatrix} \boldsymbol{M}_{bb} & \boldsymbol{M}_{bn} \\ \boldsymbol{M}_{bn}^T & \boldsymbol{M}_{nn} \end{bmatrix} \begin{bmatrix} \dot{\boldsymbol{v}}_b \\ \ddot{\boldsymbol{q}}_n \end{bmatrix} + \begin{bmatrix} \boldsymbol{C}_{bb} & \boldsymbol{C}_{bn} \\ \boldsymbol{C}_{nb} & \boldsymbol{C}_{nn} \end{bmatrix} \begin{bmatrix} \boldsymbol{v}_b \\ \dot{\boldsymbol{q}}_n \end{bmatrix} = \begin{bmatrix} \boldsymbol{F}_b \\ \boldsymbol{\tau} \end{bmatrix} \quad (1)$$

Here, $\boldsymbol{M}_{bb} \in \mathrm{R}^{6\times6}, \boldsymbol{M}_{nn} \in \mathrm{R}^{n\times n}, \boldsymbol{M}_{bn} \in \mathrm{R}^{6\times n}$ are the inertia matrices of the base, manipulator and their coupling, respectively. They are a function of the joint positions $\boldsymbol{q}_n \in \mathrm{R}^n$. Similarly, $\boldsymbol{C}_{bb} \in \mathrm{R}^{6\times6}, \boldsymbol{C}_{nn} \in \mathrm{R}^{n\times n}, \boldsymbol{C}_{bn} \in \mathrm{R}^{6\times n}, \boldsymbol{C}_{nb} \in \mathrm{R}^{n\times6}$ are sub-elements of the Coriolis/Centrifugal (CC) matrix. They depend on joint positions and velocities $\boldsymbol{q}_n, \dot{\boldsymbol{q}}_n \in \mathrm{R}^n$, and the Cartesian velocity (linear and angular), $\boldsymbol{v}_b \in \mathrm{R}^6$. The joint acceleration is $\ddot{\boldsymbol{q}}_n$ and base acceleration, $\dot{\boldsymbol{v}}_b$. The base control wrench (force and torque) is $\boldsymbol{F}_b \in \mathrm{R}^6$ and the manipulator control torques are $\boldsymbol{\tau} \in \mathrm{R}^n$.

B. Multi-rate operations of an orbital manipulator

We consider the following assumptions characterizing the multi-rate operations of the orbital manipulator.

A1. The manipulator is controlled at a high sampling frequency (eg. 1kHz) and, therefore, can be considered quasi-continuous in nature.

A2. The servicer spacecraft is controlled at a low sampling rate (eg. below 10Hz) and, therefore, can be considered discrete in nature.

A3. The manipulator has a significantly lower mass and higher control gain compared to the spacecraft, thus resulting in fast and slow dynamic time-scales, respectively.

C. Problem statement

The problem considered is a regulation task with a classical PD control law applied to both, the manipulator joints, controlled at 1 kHz, and the spacecraft base, controlled at 3 Hz. The exemplary scenario is shown in Fig. 2, where it can be seen that, compared to the quasi-continuous case (row I. of Fig. 2), the system becomes unstable with the multi-rate operation (row II. of Fig. 2). It can be seen that the low-rate (discrete) actuation of the base causes instability of the spacecraft and eventually the manipulator. The problem statement considered in the scope of this work is to design and analyze the operational bounds of a sampling-aware multi-rate combined control strategy for tackling instabilities such as the one seen here.

III. Controller design

The controller design is split between the fast dynamics of the high-rate manipulator control and the slow dynamics of the low-rate base control. The first step is to dynamically decouple the control tasks of the manipulator and servicer base. This is achieved by designing the high-rate manipulator control to compensate for the disturbances arising from the discrete control of the base. The second step is to design the spacecraft controller based on discrete-Lyapunov analysis using the decoupled dynamics.

A. High-rate manipulator control

Since the manipulator is considered to be controlled at a high-rate (eg. 1kHz), it can be modeled in continuous-time. To design the high-rate manipulator control, we inertially-decouple the manipulator from the base dynamics. This can be

IEEE Robotics and Automation Letters (RA-L) paper, presented at ICRA 2026, Vienna, Austria. Cite as RA-L paper.

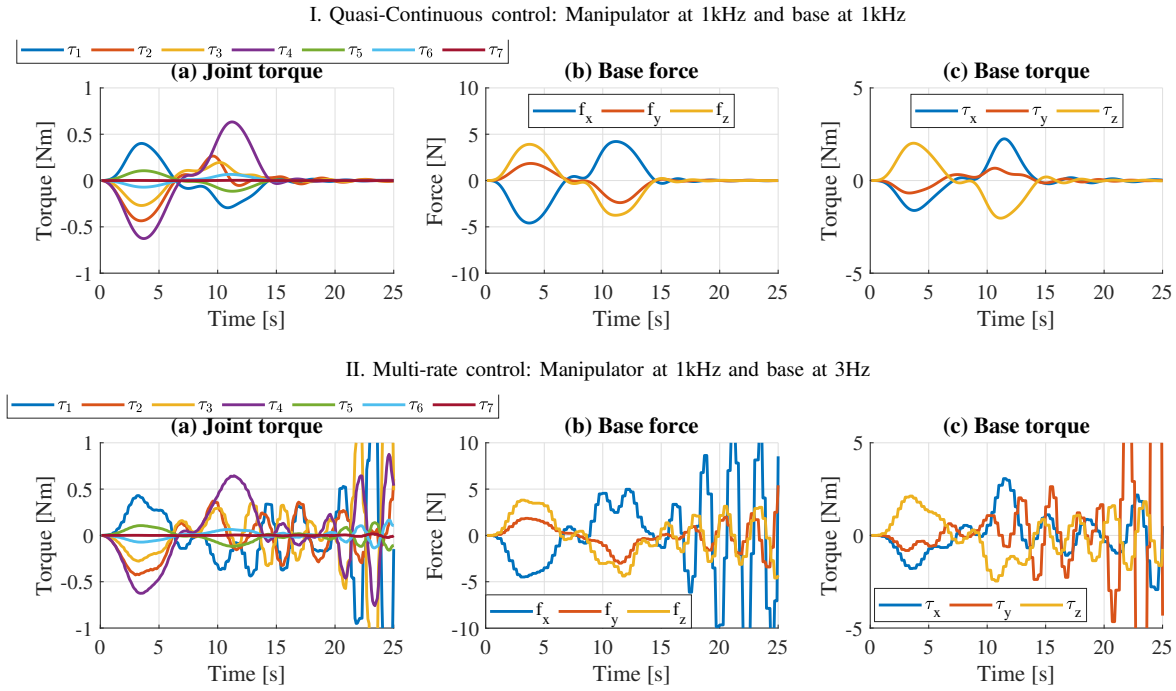

Fig. 2: *Problem statement:* Exemplary scenario showing stable vs. unstable behaviour using quasi-continuous (row I.) vs. multi-rate (row II.) control of an orbital manipulator with 7 joints. Actuator profiles compared for (a) joint torques (b) base forces and (c) base torques.

done by substituting $\dot{\boldsymbol{v}}_b$ from the top row into the manipulator dynamics in the bottom row of (1) to obtain,

$$\boldsymbol{\Lambda}_{nn}\ddot{\boldsymbol{q}}_n + \boldsymbol{\mu}_{nn}\dot{\boldsymbol{q}}_n + \boldsymbol{\mu}_{nb}\boldsymbol{v}_b = \boldsymbol{\tau} - \boldsymbol{M}_{bn}^T\boldsymbol{M}_{bb}^{-1}\boldsymbol{F}_b \tag{2}$$

where,

$$\boldsymbol{\Lambda}_{nn} = \boldsymbol{M}_{nn} - \boldsymbol{M}_{bn}^T\boldsymbol{M}_{bb}^{-1}\boldsymbol{M}_{bn},$$
$$\boldsymbol{\mu}_{nn} = \begin{bmatrix}-\boldsymbol{M}_{bn}^T\boldsymbol{M}_{bb}^{-1} & \boldsymbol{I}_n\end{bmatrix}\begin{bmatrix}\boldsymbol{C}_{bb} & \boldsymbol{C}_{bn}\\ \boldsymbol{C}_{nb} & \boldsymbol{C}_{nn}\end{bmatrix}\begin{bmatrix}-\boldsymbol{M}_{bb}^{-1}\boldsymbol{M}_{bn}\\ \boldsymbol{I}_n\end{bmatrix},$$
$$\boldsymbol{\mu}_{nb} = \boldsymbol{C}_{nb} - \boldsymbol{M}_{bn}^T\boldsymbol{M}_{bb}^{-1}\boldsymbol{C}_{bb}.$$

Here, the passivity property, $\dot{\boldsymbol{\Lambda}}_{nn} = \boldsymbol{\mu}_{nn} + \boldsymbol{\mu}_{nn}^T$ holds. The dynamics in (2) is similar to the generalized dynamics of a floating-base manipulator [20], with the difference being the non-zero momentum with base actuation. From (2) we observe that the disturbance torque on the manipulator due to the base actuation is given by the term $\boldsymbol{M}_{bn}^T\boldsymbol{M}_{bb}^{-1}\boldsymbol{F}_b$, while, the coupling torque on the manipulator due to the floating base motion is given by the Coriolis acceleration terms depending on $\boldsymbol{v}_b$. Keeping these observations in mind, we design a control law that achieves dynamic decoupling [21] of the manipulator's control task from the base by choosing,

$$\boldsymbol{\tau} = \underbrace{\boldsymbol{K}_{Pn}\Delta\boldsymbol{q}_n - \boldsymbol{K}_{Dn}\dot{\boldsymbol{q}}_n}_{\boldsymbol{\tau}_{PD}} + \underbrace{\boldsymbol{M}_{bn}^T\boldsymbol{M}_{bb}^{-1}\boldsymbol{F}_b}_{\boldsymbol{\tau}_F} + \underbrace{\boldsymbol{\mu}_{nb}\boldsymbol{v}_b}_{\boldsymbol{\tau}_v} \tag{3}$$

Here, $\boldsymbol{K}_{Pn}, \boldsymbol{K}_{Dn} \in \mathrm{R}^{n\times n}$ are the proportional and derivative (PD) gains, and $\Delta\boldsymbol{q}_n = \boldsymbol{q}_n^d - \boldsymbol{q}_n \in \mathrm{R}^n$ are the joint errors of the manipulator from the desired joint angles $\boldsymbol{q}_n^d$. The control law in (3) decouples the manipulator from the base dynamics via the terms $\boldsymbol{\tau}_F$ and $\boldsymbol{\tau}_v$. It is worth noting that the control law in (3) is consistent with prioritizing the manipulator task by projecting the base control task in its nullspace [22].

Proposition 1. *Consider the system* (1) *with the control law* (3)*. Assume that the stiffness and damping gains* $\boldsymbol{K}_{Pn}$ *and* $\boldsymbol{K}_{Dn}$ *are symmetric and positive-definite. Then, the control law in* (3) *results in the equilibrium* $\Delta\boldsymbol{q}_n, \dot{\boldsymbol{q}}_n = \boldsymbol{0}$ *being asymptotically stable.*

Proof. Consider the continuous-time positive definite candidate Lyapunov function,

$$V_n = \frac{1}{2}\dot{\boldsymbol{q}}_n^T\boldsymbol{\Lambda}_{nn}\dot{\boldsymbol{q}}_n + \frac{1}{2}\Delta\boldsymbol{q}_n^T\boldsymbol{K}_{Pn}\Delta\boldsymbol{q}_n \tag{4}$$

Its time-derivative along a trajectory governed by the dynamics in (2) results in,

$$\dot{V}_n = \dot{\boldsymbol{q}}_n^T(\boldsymbol{\tau} - \boldsymbol{K}_{Pn}\Delta\boldsymbol{q}_n - \boldsymbol{M}_{bn}^T\boldsymbol{M}_{bb}^{-1}\boldsymbol{F}_b - \boldsymbol{\mu}_{nb}\boldsymbol{v}_b) \tag{5}$$

where, the passivity property $\dot{\boldsymbol{\Lambda}}_{nn} = \boldsymbol{\mu}_{nn} + \boldsymbol{\mu}_{nn}^T$ is used. Therefore, substituting the control law (3) results in $\dot{V}_n = -\dot{\boldsymbol{q}}_n^T\boldsymbol{K}_{Dn}\dot{\boldsymbol{q}}_n$ which is negative semi-definite. From this we conclude stability and boundedness of the manipulator states. Further, using LaSalle's invariance principle, we conclude asymptotic stability of the equilibrium $\Delta\boldsymbol{q}_n, \dot{\boldsymbol{q}}_n = \boldsymbol{0}$. □

B. Low-rate base control

The proposed approach first discretizes the base dynamics in the set of the converged manipulator errors. A sample-and-hold discrete controller designed using the discretized dynamics will result in energy leaks [23] due to a mismatch in the physical and virtual energies of the continuous plant and discrete controller between sampling instants. Therefore, a discrete Lyapunov-based controller is designed to compensate these sampling effects up to the first order.

IEEE Robotics and Automation Letters (RA-L) paper, presented at ICRA 2026, Vienna, Austria. Cite as RA-L paper.

We recall the base dynamics from (1) and consider it in the set that the manipulator states are converged, i.e. $\Delta \boldsymbol{q}_n, \dot{\boldsymbol{q}}_n = \boldsymbol{0}$.

$$\boldsymbol{M}_{bb}\dot{\boldsymbol{v}}_b + \boldsymbol{C}_{bb}\boldsymbol{v}_b = \boldsymbol{F}_b \tag{6}$$

Note that the passivity property, $\dot{\boldsymbol{M}}_{bb} = \boldsymbol{C}_{bb} + \boldsymbol{C}_{bb}^T$ holds. The base dynamics in (6) with zero-order-hold on the control input can be discretized using the Taylor series expansion [24] as,

$$\boldsymbol{v}_b[k+1] = \boldsymbol{v}_b[k] + h\dot{\boldsymbol{v}}_b[k] + \frac{1}{2!}h^2\ddot{\boldsymbol{v}}_b[k] + \dots \tag{7}$$

where h is the sampling time corresponding to the actuation rate of the base, and $\dot{\boldsymbol{v}}_b[k]$ and its higher derivatives are computed from (6). To compensate for the sampling effect up to the first-order of h, we propose to design the low-rate base control law by considering $\boldsymbol{F}_b$ of the form

$$\boldsymbol{F}_b[k] = \boldsymbol{F}_{b0}[k] + h\boldsymbol{F}_{b1}[k] \tag{8}$$

where, $\boldsymbol{F}_{b0}$ is the zero-order state-feedback control and $\boldsymbol{F}_{b1}$ is the first-order control law that compensates first-order sampling effects. Therefore, we choose

$$\begin{aligned}\boldsymbol{F}_{b0}[k] = \;& \boldsymbol{E}\boldsymbol{K}_{Pb}\Delta\boldsymbol{x}_b - \boldsymbol{K}_{Db}\boldsymbol{v}_b \\ \boldsymbol{F}_{b1}[k] = \;& -\frac{1}{2}\boldsymbol{K}_{Db}^T\boldsymbol{M}_{bb}^{-1}\boldsymbol{E}\boldsymbol{K}_{Pb}\Delta\boldsymbol{x}_b + \frac{1}{2}\dot{\boldsymbol{E}}\boldsymbol{K}_{Pb}\Delta\boldsymbol{x}_b \\ & -\frac{1}{2}(\boldsymbol{E}\boldsymbol{K}_{Pb}\boldsymbol{E}^T - \boldsymbol{K}_{Db}^T\boldsymbol{M}_{bb}^{-1}\boldsymbol{C}_{bb} - \boldsymbol{K}_{Db}^T\boldsymbol{M}_{bb}^{-1}\boldsymbol{K}_{Db})\boldsymbol{v}_b\end{aligned} \tag{9}$$

where $[k]$ has been omitted for all quantities on the right-hand-side for brevity. Here, $\boldsymbol{K}_{Pb}, \boldsymbol{K}_{Db} \in \mathrm{R}^{6\times 6}$ are the zero-order PD gains. We consider the Cartesian pose error (position and orientation) of the base, $\Delta\boldsymbol{x}_b \in \mathrm{R}^6$, such that $\Delta\dot{\boldsymbol{x}}_b = -\boldsymbol{E}^T\boldsymbol{v}_b$ [1]. The design of $\boldsymbol{F}_{b0}$ and $\boldsymbol{F}_{b1}$ as in (9) is a consequence of discrete-Lyapunov analysis (detailed in the proof of Proposition 2 ahead) that reduces the sampling effects to the order of $\mathcal{O}(h^2)$. Finally, (8) with (9) can be equivalently re-arranged as

$$\boldsymbol{F}_b[k] = (\underbrace{\boldsymbol{E}\boldsymbol{K}_{Pb} + h\boldsymbol{K}_{Pb1}}_{\bar{\boldsymbol{K}}_{Pb}})\Delta\boldsymbol{x}_b - (\underbrace{\boldsymbol{K}_{Db} + h\boldsymbol{K}_{Db1}}_{\bar{\boldsymbol{K}}_{Db}})\boldsymbol{v}_b \tag{10}$$

$$\text{where,}\quad \boldsymbol{K}_{Pb1} = \frac{1}{2}(\dot{\boldsymbol{E}}\boldsymbol{K}_{Pb} - \boldsymbol{K}_{Db}\boldsymbol{M}_{bb}^{-1}\boldsymbol{E}\boldsymbol{K}_{Pb}),$$

$$\boldsymbol{K}_{Db1} = \frac{1}{2}(\boldsymbol{E}\boldsymbol{K}_{Pb}\boldsymbol{E}^T - \boldsymbol{K}_{Db}\boldsymbol{M}_{bb}^{-1}\boldsymbol{C}_{bb} - \boldsymbol{K}_{Db}\boldsymbol{M}_{bb}^{-1}\boldsymbol{K}_{Db})$$

Note that $\bar{\boldsymbol{K}}_{Pb}$ and $\bar{\boldsymbol{K}}_{Db}$ are the sampling-aware PD gains that tend to the classical continuous-time PD gains when $h \to 0$. A schematic of the multi-rate combined controller is summarized in Fig. 3.

Proposition 2. *Consider the dynamics in* (6) *in the set* $\Delta\boldsymbol{q}, \dot{\boldsymbol{q}} = \boldsymbol{0}$ *discretized using the Taylor series as per* (7) *with the control law in* (10)*. The stiffness and damping gains* $\boldsymbol{K}_{Pb}$ *and* $\boldsymbol{K}_{Db}$ *are symmetric and positive-definite. Then, neglecting higher-order terms, the control law in* (10) *results in the equilibrium* $\Delta\boldsymbol{x}_b, \boldsymbol{v}_b = 0$ *being asymptotically stable conditionally to the set* $\Delta\boldsymbol{q}_n, \dot{\boldsymbol{q}}_n = \boldsymbol{0}$.

[1]Here, $\boldsymbol{E} = \mathrm{diag}(\boldsymbol{I}_3, \frac{1}{2}(\Delta\eta\boldsymbol{I}_3 + S(\Delta\boldsymbol{\epsilon})))$, where $\Delta\eta, \Delta\boldsymbol{\epsilon}$ are the scalar, vector parts of the error quaternion and $S(\cdot)$ is the skew-symmetric cross-product operator [25].

Proof. Consider the following positive definite candidate Lyapunov function

$$V_b = \frac{1}{2h}\boldsymbol{v}_b^T\boldsymbol{M}_{bb}\boldsymbol{v}_b + \frac{1}{2h}\Delta\boldsymbol{x}_b^T\boldsymbol{K}_{Pb}\Delta\boldsymbol{x}_b \tag{11}$$

in the set of the manipulator errors converged i.e. $\Delta\boldsymbol{q}_n, \dot{\boldsymbol{q}}_n = \boldsymbol{0}$. The Lyapunov difference equation of (11) in discrete-time can be written as,

$$\begin{aligned}&V_b[k+1] - V_b[k] = \\ &+ \frac{1}{2h}\boldsymbol{v}_b^T[k+1]\boldsymbol{M}_{bb}[k+1]\boldsymbol{v}_b[k+1] - \frac{1}{2h}\boldsymbol{v}_b^T[k]\boldsymbol{M}_{bb}[k]\boldsymbol{v}_b[k] \\ &+ \frac{1}{2h}\Delta\boldsymbol{x}_b^T[k+1]\boldsymbol{K}_{Pb}\Delta\boldsymbol{x}_b[k+1] - \frac{1}{2h}\Delta\boldsymbol{x}_b^T[k]\boldsymbol{K}_{Pb}\Delta\boldsymbol{x}_b[k]\end{aligned} \tag{12}$$

Further, consider the expansions $\boldsymbol{M}_{bb}[k+1] = \boldsymbol{M}_{bb}[k] + h\dot{\boldsymbol{M}}_{bb}[k] + \frac{1}{2!}h^2\ddot{\boldsymbol{M}}_{bb}[k] + \dots$ and $\Delta\boldsymbol{x}_b[k+1] = \Delta\boldsymbol{x}_b[k] + h\Delta\dot{\boldsymbol{x}}_b[k] + \frac{1}{2!}h^2\Delta\ddot{\boldsymbol{x}}_b[k] + \dots$ Applying (6)-(7) and the above expansions to (12), followed by some tedious but straightforward simplifications result in

$$\begin{aligned}&V_b[k+1] - V_b[k] = \\ &(\boldsymbol{v}_b - \frac{h}{2}\boldsymbol{M}_{bb}^{-1}\boldsymbol{C}_{bb}\boldsymbol{v}_b + \frac{h}{2}\boldsymbol{M}_{bb}^{-1}\boldsymbol{F}_b)^T(\boldsymbol{F}_b - \boldsymbol{E}\boldsymbol{K}_{Pb}\Delta\boldsymbol{x}_b) \\ &+ \frac{h}{2}\boldsymbol{v}_b^T\boldsymbol{E}\boldsymbol{K}_{Pb}\boldsymbol{E}^T\boldsymbol{v}_b - \frac{h}{2}\boldsymbol{v}_b^T\dot{\boldsymbol{E}}\boldsymbol{K}_{Pb}\Delta\boldsymbol{x}_b + \mathcal{O}(h^2)\end{aligned} \tag{13}$$

where the passivity property $\dot{\boldsymbol{M}}_{bb} = \boldsymbol{C}_{bb} + \boldsymbol{C}_{bb}^T$ has been used. Considering $\boldsymbol{F}_b$ as in (8) and $\boldsymbol{F}_{b0}$ as in (9), we can obtain $\boldsymbol{F}_{b1}$ as in (9) to yield,

$$V_b[k+1] - V_b[k] = -\bar{\boldsymbol{v}}_b^T\boldsymbol{K}_{Db}\bar{\boldsymbol{v}}_b + \mathcal{O}(h^2) \tag{14}$$

where, $\bar{\boldsymbol{v}}_b = \boldsymbol{v}_b - \frac{h}{2}\boldsymbol{M}_{\boldsymbol{bb}}^{-1}\boldsymbol{C}\boldsymbol{v}_b + \frac{h}{2}\boldsymbol{M}_{bb}^{-1}\boldsymbol{F}_{b0}$. Neglecting higher order terms, the control law (10) for $\boldsymbol{F}_b$ yields (14) negative semi-definite, showing boundedness of the considered states. Further, applying LaSalles's invariance principle for discrete systems [26] it can be shown that all trajectories in the set $\Delta\boldsymbol{q}_n, \dot{\boldsymbol{q}}_n = \boldsymbol{0}$ will converge to the equilibrium $\Delta\boldsymbol{x}_b, \boldsymbol{v}_b = \boldsymbol{0}$. This allows to conclude that the equilibrium $\Delta\boldsymbol{x}_b, \boldsymbol{v}_b = \boldsymbol{0}$ is conditionally stable in the set $\Delta\boldsymbol{q}_n, \dot{\boldsymbol{q}}_n = \boldsymbol{0}$, neglecting higher order terms. □

Note that for combined stability, V_n can be considered as in (4) to be the semi-definite Lyapunov function of the complete system. In addition, using the conditional stability analysis in Proposition 2 and neglecting higher-order terms, combined stability can be concluded similar to [27] for discrete-time systems. Note that the proof of stability here does not imply sequential convergence, rather it is a simultaneous convergence of hierarchical tasks [22]. In other words, the hierarchy is not referring to time of convergence but the decoupling via the nullspace of the base disturbance on the manipulator.

Discussion

All terms in (13) besides $\boldsymbol{v}_b^T(\boldsymbol{F}_b - \boldsymbol{E}\boldsymbol{K}_{Pb}\Delta\boldsymbol{x}_b)$ are the sampling effects in discrete time of the continuous-time plant. This can be seen as the energy leak described in [23] occuring due to the discrete controller's inability to react between sampling instants. The proposed discrete controller in (10) reduces this energy leak to the (negligible) order of $\mathcal{O}(h^2)$.

IEEE Robotics and Automation Letters (RA-L) paper, presented at ICRA 2026, Vienna, Austria. Cite as RA-L paper.

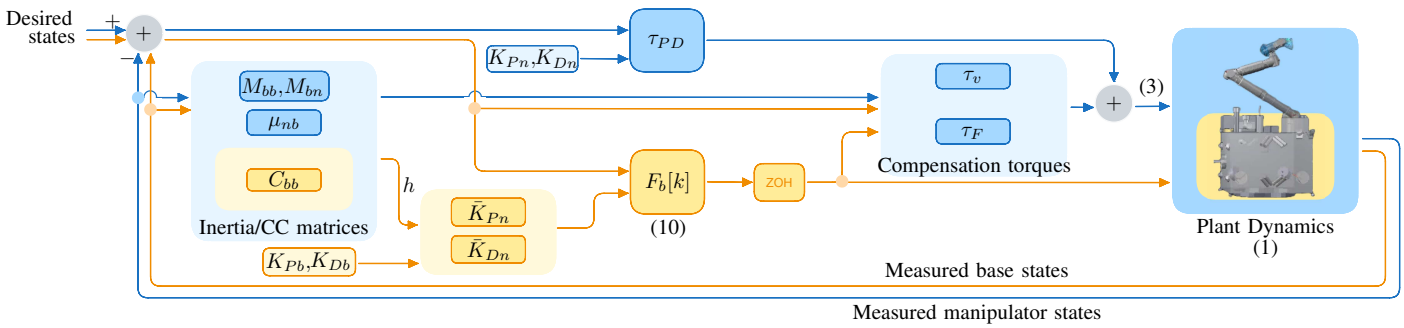

Fig. 3: Block diagram of the proposed combined control of the orbital manipulator shows how the high-rate manipulator control (3) and low-rate base control (10) are computed. The blocks/signals in blue and yellow associate with high- and low-rate control, respectively.

The rationale for targeting the Lyapunov difference equation as in (14) lies in a key observation that (13) can alternatively be seen as,

$$V_b[k+1] - V_b[k] = \underbrace{(\boldsymbol{v}_b + \frac{h}{2}\dot{\boldsymbol{v}}_b)}_{\approx \boldsymbol{v}_b[k+\frac{1}{2}]}{}^T (\boldsymbol{F}_b - \underbrace{(\boldsymbol{E} + \frac{h}{2}\dot{\boldsymbol{E}})}_{\approx \boldsymbol{E}[k+\frac{1}{2}]} \boldsymbol{K}_{Pb} \underbrace{(\Delta \boldsymbol{x}_b - \frac{h}{2}\boldsymbol{E}^T \boldsymbol{v}_b)}_{\approx \Delta \boldsymbol{x}_b[k+\frac{1}{2}]}) + \mathcal{O}(h^2) \tag{15}$$

while neglecting higher-order terms. This shows that the first-order approximation of the Lyapunov difference equation can be captured by the first-order approximation of the states at mid-sampling instant $[k + \frac{1}{2}]$. Applying the control law in (10) is equivalent to $\boldsymbol{F}_b = \boldsymbol{F}_{b0} + \frac{h}{2}\dot{\boldsymbol{F}}_{b0} \approx \boldsymbol{F}_b[k + \frac{1}{2}]$, the first-order approximation of the continuous-domain controller at mid-sampling instant, where $\boldsymbol{F}_{b1} = \frac{1}{2}\dot{\boldsymbol{F}}_{b0}$.

IV. Evaluation of Sampled-Data Controller on a Low-Dimensional Benchmark

In this section, we validate the novel discrete controller applied to a 1-DoF double-integrator plant for simplicity and clarity. This gives us an insight into the operational bounds of the discrete controller enhanced to tackle first-order sampling effects. This shall provide a baseline for anticipating the controller's performance in the nonlinear multi-DoF case.

The results of the discrete-controller in (10) applied to a 1-DoF case are presented for an exemplary plant with mass $M = 5\text{kg}$ and stiffness $K_P = 25\text{N/m}$. A comparison of the stability to a step-input is performed between the 0th order ($\boldsymbol{F}_{b0}$) and 1st order ($\boldsymbol{F}_{b0} + h\boldsymbol{F}_{b1}$) PD control law for 4000 data points across a grid of damping and sampling ratios. Stability is determined by the location of the poles inside the unit circle. The damping ratio equals $\zeta = K_D/(2\sqrt{K_P M})$ and the sampling ratio equals ω_s/ω_n, where $\omega_s = 2\pi/h$ is the sampling frequency[2] and $\omega_n = \sqrt{K_P/M}$ is the natural frequency. Note that here we use the sampling frequency normalized by the natural frequency so as to make the result agnostic to the mass and stiffness chosen.

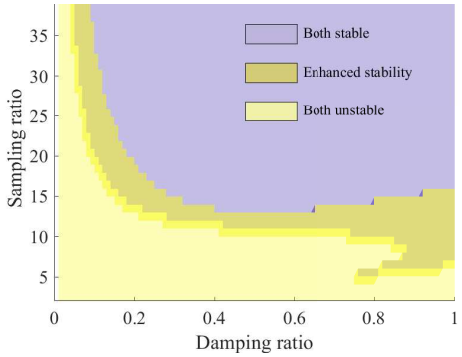

Fig. 4: *Low-rate discrete-control for 1-DoF plant:* Region of stability for the 0th order and 1st order PD control law.

The increase in the boundary of stability is shown in Fig. 4 by the overlapping area between violet and yellow regions. In this overlapping region, the 1st order PD controller stabilizes instability seen with 0th order PD. We can observe that regions with either very low sampling ratios or very low damping ratios are more prone to instability. In Fig. 4 , the range of sampling ratio above 15 and damping ratio above 0.4 results in a stable system. This evaluation facilitates the tuning of the control gains a-priori and anticipate boundaries of stability.

V. Simulation Results for Multi-Rate Combined Control of an Orbital Manipulator

This section presents simulation results of the proposed multi-rate combined controller applied to the multi-DoF case of an orbital manipulator. First, we show the effectiveness of the proposed multi-rate combined control in tackling the instability presented in the problem statement, Fig. 2. Second, we highlight the significance of the compensation torques designed for the high-rate manipulator control. Lastly, we compare the proposed 1st order multi-rate combined control against the 0th order control scheme for 99 data points across randomized initial poses of the manipulator and base.

The simulation setup in Fig. 1 (a) uses an orbital manipulator from the EROSS IOD mission [28]. The manipulator considered is the 7-DoF CAESAR arm. The servicing spacecraft considered weighs 360kg and its inertia elements in the spacecraft body frame are $I_{xx} = 210, I_{yy} = 77, I_{zz} = 212, I_{xy} = 1.9, I_{xz} = 1.7, I_{yz} = 3.2\ \text{kgm}^2$. The manipulator is controlled at a high-rate of 1kHz and the servicer spacecraft is controlled at a low-rate of 3Hz, i.e. $h = 0.33\text{s}$. The initial velocity (linear and angular) of the servicer and client is zero. The initial manipulator pose is $[90, 75, 0, 160, 0, 0, 120]\text{deg}$.

[2]To avoid signal aliasing, the lower limit for sampling is known to be twice the natural frequency.

IEEE Robotics and Automation Letters (RA-L) paper, presented at ICRA 2026, Vienna, Austria. Cite as RA-L paper.

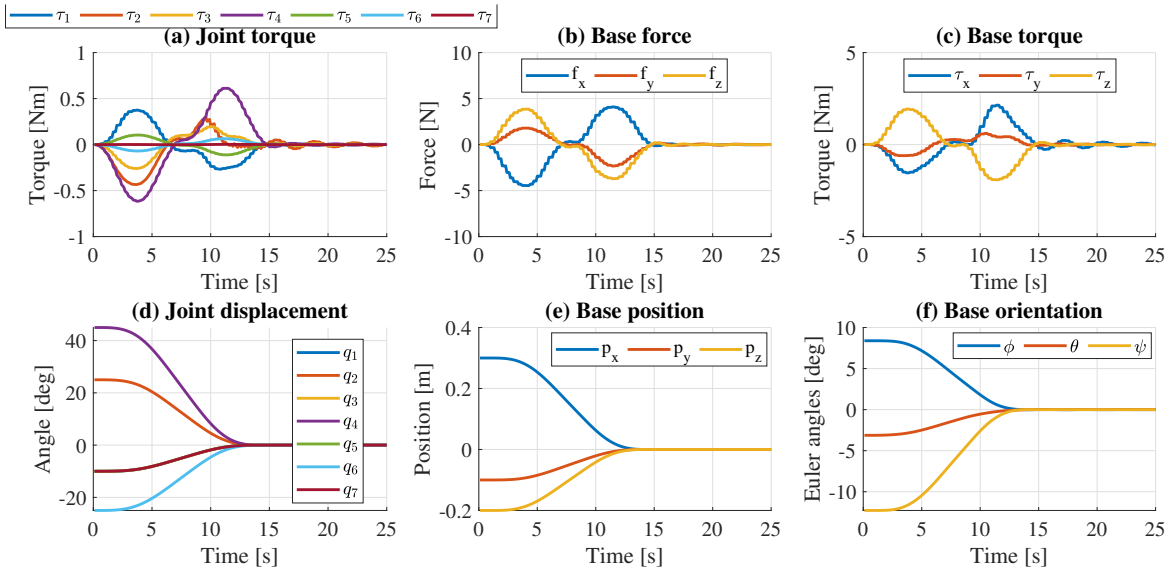

Fig. 5: Stabilized manipulator and base actuation profiles and trajectories using proposed method for scenario in problem statement, Fig. 2. For ease of presentation, Euler angles (ϕ, θ, ψ in the XYZ convention) are reported here.

1) Problem statement scenario with proposed method: The example scenario shown in the problem statement Fig. 2 considers a base displacement of $[-0.3, 0.1, 0.2]$m and $[-8, 4, 12]$deg, and manipulator displacement of $[10, -25, 10, -45, 10, 25, 10]$deg. A smooth trajectory is interpolated from the initial to the final setpoint. An overlay of the initial and final poses of this maneuver are shown in Fig. 1 (a). The gains for the manipulator control are set to $\boldsymbol{K}_{Pn}$ as $\mathrm{diag}(400, 800, 400, 400, 100, 100, 40)$Nm/rad and $\boldsymbol{K}_{Dn}$ as $\mathrm{diag}(300, 300, 200, 200, 20, 20, 10)$Nms/rad. The 0-order gains for the spacecraft control are set to $\boldsymbol{K}_{Pb}$ as $\mathrm{diag}([2500, 2500, 2500]\mathrm{N/m}, [1000, 1000, 1000]\mathrm{Nm/rad})$, $\boldsymbol{K}_{Db}$ as $\mathrm{diag}([250, 250, 250]\mathrm{Ns/m}, [100, 100, 100]\mathrm{Nms/rad})$.

The result of applying the low-rate 0th order PD control on the base and high-rate PD control on the manipulator without any decoupling was shown in the problem statement in Fig. 2. The result with the proposed multi-rate combined control laws in (3) and (10) is now presented in Fig. 5 for comparison. It can be seen from Fig. 5 that the proposed method stabilizes the scenario in the problem statement, which lay in a region of low sampling ratio ($\approx$7.5) and damping ratio ($\approx$0.12). The mean absolute error between the total Lyapunov difference equation in (12) and the O(h) approximation in (15) is bounded below 0.25J/s. Further, omitting compensation torques ($\boldsymbol{\tau}_F$ and $\boldsymbol{\tau}_v$) in (3) only result in minor joint vibration, seen in Fig. 6 (a).

2) Comparison to passivity-based control [19]: The proposed method has been compared with the passivity based approach presented in [19] under identical conditions at 8 Hz. A comparison of the impulse (integral of force and torque as a measure of the efficiency) is shown in Fig. 6(b) . The method in [19] has maximum values of 74 Ns and 33 Nms at the end of the maneuver against the lower values of 46 Ns and 20 Nms of the proposed method. The method in [19] is based on observation first (observe energy) and action later (dissipate active energy with passivity control). This translates

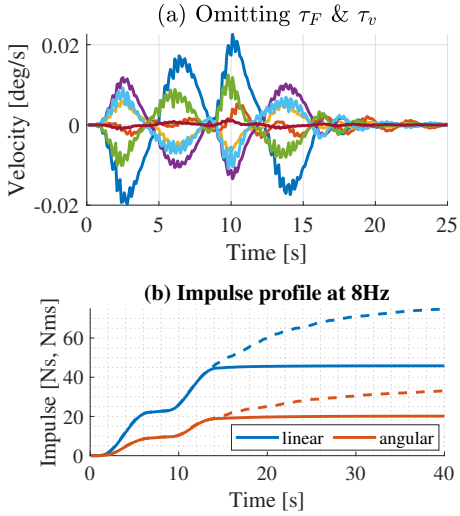

Fig. 6: (a) Manipulator joint velocities while omitting compensation torques with discrete base control. (b) Impulse profile compared with [19] (in dashed lines) versus proposed 1st order PD (in solid lines).

in more impulse (consumption) for the system. In contrast, the proposed method, acts a-priori (i.e. from a theoretical deduction) to reduce the system activity.

3) Grid search with randomized initial conditions: To cover a wider spectrum of dynamic motions a set of simulations were performed for randomized poses sampled from a uniform distribution across a grid of damping [29] and sampling ratios for the base controller. The grid considers damping ratios between $[0.1, 0.9]$ in steps of 0.1 and sampling ratios between $[3, 33]$ in steps of 3. Considering a natural frequency of $\omega_n = \pi$rad/s, this translates to a range of $[1.5, 16.5]$Hz in steps of 1.5Hz for the base control. The initial pose of the manipulator was sampled from a range of $\pm[130, 40, 130, 130, 130, 130, 130]$deg and the displacement was randomly chosen as $\pm$50deg per joint. The base displacement was sampled along the surface

IEEE Robotics and Automation Letters (RA-L) paper, presented at ICRA 2026, Vienna, Austria. Cite as RA-L paper.

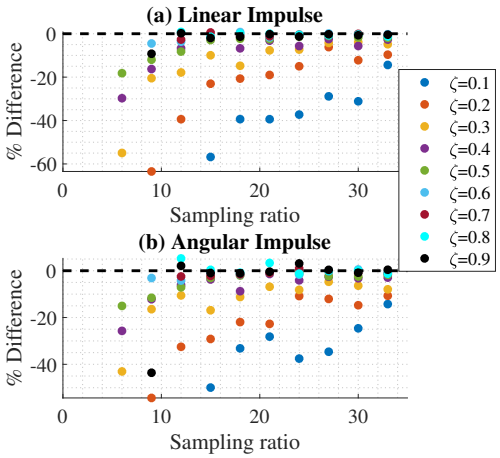

Fig. 7: Difference in (a) linear and (b) angular impulse utilized by the 0th order vs. proposed 1st order multi-rate combined control shown across increasing sampling and damping ratios.

of spheres of radii 0.5m and 30deg. Therefore, the norm of manipulator and base displacements were considered the same (regardless of the initial pose and direction of displacement) for a fair comparison of the impulse utilized by the different maneuvers. For sensitivity analysis, model parameters are perturbed up to 20% in the mass, inertia and center-of-mass. The 0-order stiffness gain of the base controller is chosen as $\boldsymbol{K}_{Pb} = \omega_n^2/\boldsymbol{M}_{bb}(\boldsymbol{q}(0))$ using the initial pose $\boldsymbol{q}(0)$. The manipulator gains are similarly tuned as $\boldsymbol{K}_{Pn} = \omega_n^2/\boldsymbol{M}_{nn}(\boldsymbol{q}(0))$ and $\boldsymbol{K}_{Dn}$ set to a damping ratio of 0.7, which must not be confused with the range of damping ratios of the base controller considered for the analysis.

For each data point thus generated, 80 data points out of 99 were observed to be stable for both controllers. A comparison of the impulse utilized for the maneuvers is shown in Fig. 7. Here, we observe that 93% and 89% of stable data points led to a reduction in the linear and angular impulse consumed, respectively. The mean and standard deviation of the reduction was observed to be 9.64 Ns and 14.22 Ns in linear, and 9.22 Nms and 13.21 Nms in angular impulse, respectively. The remaining stable data points with high damping ratio of $\zeta > 0.6$ have a comparable/marginal increase in the impulse consumed. Thus, the proposed method is observed to perform better particularly in regions of low damping ratios.

VI. Hardware-in-the-Loop Results for Multi-Rate Combined Control

The HIL platform uses the servicer robot of the DLR, OOS-Sim (250Hz) able to simulate 0-g dynamics at 1kHz and the intrinsic time delay of the facility is 4ms [30]. The HIL setup (see Fig. 1) is equipped with a 7-DoF LWR manipulator. The servicing spacecraft considered weighs 200kg and its inertia elements in the spacecraft body frame are $I_{xx} = 100, I_{yy} = 100, I_{zz} = 100, I_{xy} = 3, I_{xz} = 0, I_{yz} = 0$ kgm^2. The manipulator is controlled at a high-rate of 1kHz and the servicer spacecraft is controlled at a low-rate of $5\text{Hz}(h = 0.2\text{s})$.

The gains for the manipulator control are $\boldsymbol{K}_{Pn}$=diag$(150, 150, 135, 100, 50, 50, 50)\text{Nm/rad}$ and $\boldsymbol{K}_{Dn}$=diag$(20, 30, 1, 1, 1, 1, 1)\text{Nms/rad}$. The 0-order gains for the spacecraft control are set to a damping ratio of 0.7 with $\boldsymbol{K}_{Pb}$ =diag$([220, 220, 220]\text{N/m}, [120, 130, 110]\text{Nm/rad})$ and $\boldsymbol{K}_{Db}$=diag$([305, 305, 305]\text{Ns/m}, [170, 180, 150]\text{Nms/rad})$. Thus, a control rate of 5Hz results in a sampling ratio ≈ 31.

The scenario considers a close-proximity maneuver of the servicer spacecraft towards the client along with the manipulator. An overlay of the initial and final poses of this maneuver are shown in Fig. 1 (b). The desired displacement for the base is $[0.1, 0.0, -0.1]\text{m}$ and $[-10, 0, 0]\text{deg}$, and for the manipulator is $[0, -47, 4, -28, -1, -15, 3]\text{deg}$. A smooth trajectory is interpolated from the initial to the final setpoint.

The result of applying the proposed multi-rate combined control laws in (3) and (10) to the scenario is presented in Fig. 8. The proposed multi-rate control is seen to stabilize the combined motion of the spacecraft base and manipulator to reach the desired setpoint with a maximum error of 0.9deg per joint and $10^{-4}\text{m}, 0.1\text{deg}$ in norm for the base. The steady-state residual torques in Fig. 8 (a) arise from the joint friction. The discrete nature of the base actuation at 5Hz can be observed from the staggered profile of the force and torques in Fig. 8 (b) and (c). The final linear and angular impulses for this scenario are reduced by 1% and 4% respectively by using the proposed method versus the 0th order PD control.

The same maneuver was repeated with lower sampling rates of $3\text{Hz}, 2\text{Hz}$ and 1Hz for the base control. The recorded impulse reduction is reported in Table I comparing the proposed 1st order PD to the 0th order control. It can be seen from the values that the proposed method was more efficient for the conducted experiments and the nonlinearity of the dynamics is evident from the nonlinear reduction of impulse across different base control rates.

TABLE I: *HIL experiments:* Efficiency of base actuation at different sampling rates with damping ratio of 0.7. *Percentage reduction in impulse compared using the 1st order versus 0th order PD.

Base rate	Sampling ratio	Linear* [%]	Angular* [%]
5 Hz	31	-1	-4
3 Hz	19	-7	-11
2 Hz	13	-3	-7
1 Hz	6	-21	-34

VII. Conclusions

In this paper, we proposed a multi-rate controller that addresses the combined control problem encountered in the operation of an orbital manipulator. This is achieved through two main innovations - the design of a discrete controller that considers the servicer's low sampling rate, and a combined control strategy that separates the manipulator's high-rate control from the spacecraft's discrete control. The proposed (control) concept is first validated in simulation using a one-DoF benchmark showing the enhancement of the boundary of stability with the proposed method. Second, simulations are performed using a multi-DoF orbital manipulator to compare the impulse utilization as a measure of efficiency. The method is further validated using a hardware-in-the-loop setup. Extensions of the method to Cartesian control or, to quantized input and time delay with [3] and [31], which rely on power ports and energy measurements, may be scope for future work.

IEEE Robotics and Automation Letters (RA-L) paper, presented at ICRA 2026, Vienna, Austria. Cite as RA-L paper.

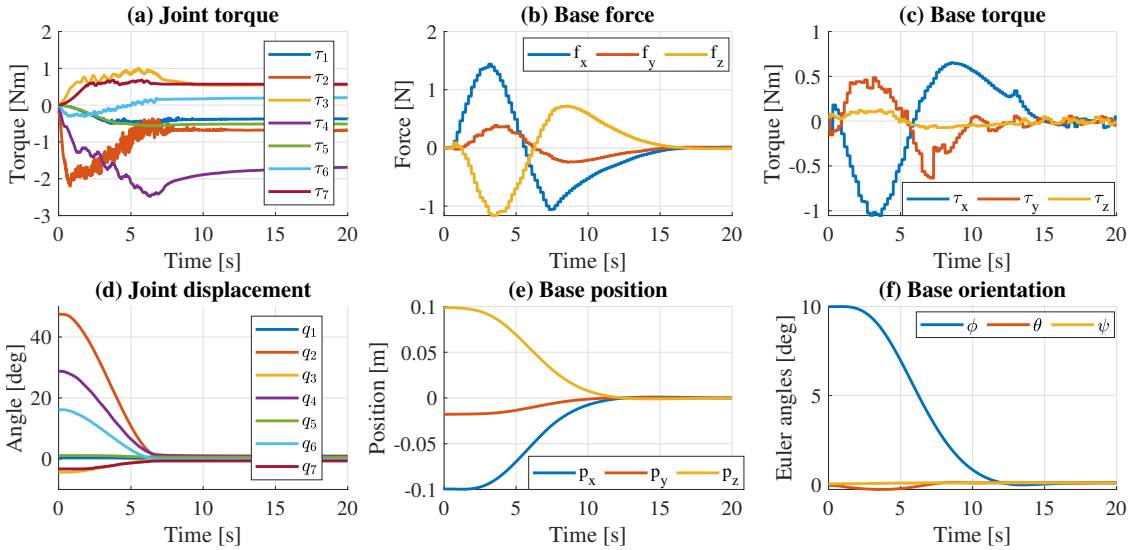

Fig. 8: *HIL experiment:* Manipulator and base actuation profiles and trajectories for close-proximity maneuver performed using proposed method with low-rate (5Hz) base control and high-rate (1kHz) manipulator control. For ease of presentation, Euler angles are reported here.

REFERENCES

[1] P. Colmenarejo *et al.*, "Methods and outcomes of the comrade project - design of robust combined control for robotic spacecraft and manipulator in servicing missions," in *69th International Astronautical Congress*, Sept 2018.

[2] N. Diolaiti, G. Niemeyer, F. Barbagli, and J. Salisbury, "Stability of haptic rendering: Discretization, quantization, time delay, and coulomb effects," *IEEE Transactions on Robotics*, vol. 22, pp. 256–268, 2006.

[3] M. De Stefano, R. Balachandran, and C. Secchi, "A passivity-based approach for simulating satellite dynamics with robots: Discrete-time integration and time-delay compensation," *IEEE Transactions on Robotics*, vol. 36, no. 1, pp. 189–203, 2020.

[4] V. Tanasa, S. Monaco, and D. Normand-Cyrot, "Backstepping control under multi-rate sampling," *IEEE Transactions on Automatic Control*, vol. 61, no. 5, pp. 1208–1222, 2016.

[5] K. Cao, C. Wen, and J. Gu, "Sampled-data stabilization of nonholonomic chained form systems with multi-rate samplings," in *IECON 49th Annual Conference of the IEEE Industrial Electronics Society*, 2023, pp. 1–6.

[6] M. Mattioni *et al.*, "On feedback passivation under sampling," in *American Control Conference (ACC)*, 2021, pp. 3578–3583.

[7] J. Jia, H. Dai, J. Li, and X. Yang, "Global stabilization by means of a new sampled-data control scheme for a class of nonlinear time-delay systems," in *9th International Conference on Information Science and Technology (ICIST)*, 2019, pp. 24–28.

[8] J. Jia, W. Chen, and H. Dai, "Multi-rate sampled-data control for a class of nonlinear systems via input-lyapunov matching," in *36th Chinese Control Conference (CCC)*, 2017, pp. 868–871.

[9] M. Mattioni, A. Moreschini, S. Monaco, and D. Normand-Cyrot, "Discrete-time energy-balance passivity-based control," *Automatica*, vol. 146, p. 110662, 2022.

[10] T. Hulin, A. Albu-Schäffer, and G. Hirzinger, "Passivity and stability boundaries for haptic systems with time delay," *IEEE Transactions on Control Systems Technology*, vol. 22, no. 4, pp. 1297–1309, 2014.

[11] I. Napoli and M. Pontani, "Discrete-variable-thrust guidance for orbital rendezvous based on feedback linearization," *Aerotecnica Missili & Spazio*, vol. 101, no. 4, pp. 351–360, 2022.

[12] M. Homayounzade, "Adaptive robust nonlinear control of spacecraft formation flying: a novel disturbance observer-based control approach," *International Journal of Dynamics and Control*, vol. 10, no. 5, pp. 1471–1484, 2022.

[13] M. Pontani and M. Pustorino, "Low-thrust lunar capture leveraging nonlinear orbit control," *The Journal of the Astronautical Sciences*, vol. 70, no. 5, p. 28, 2023.

[14] Y. Ikeda, "Discrete-time nonlinear attitude tracking control of spacecraft," in *11th IEEE Asian Control Conference (ASCC)*, 2017, pp. 617–622.

[15] Y. Wu *et al.*, "Adaptive fault-tolerant control for spacecraft formation under external disturbances with guaranteed performance," *Advances in Space Research*, vol. 72, no. 5, pp. 1583–1592, 2023.

[16] L. Chen *et al.*, "Characteristic model-based discrete-time sliding mode control for spacecraft with variable tilt of flexible structures," *IEEE/CAA Journal of Automatica Sinica*, vol. 3, no. 1, pp. 42–50, 2016.

[17] C. D. Petersen, F. Leve, and I. Kolmanovsky, "Model predictive control of an underactuated spacecraft with two reaction wheels," *Journal of Guidance, Control, and Dynamics*, vol. 40, no. 2, pp. 320–332, 2017.

[18] P. Taborda, H. Matias, D. Silvestre, and P. Lourencco, "Convex mpc and thrust allocation with deadband for spacecraft rendezvous," *IEEE Control Systems Letters*, vol. 8, pp. 1132–1137, 2024.

[19] M. De Stefano *et al.*, "Multi-rate tracking control for a space robot on a controlled satellite: A passivity-based strategy," *IEEE Robotics and Automation Letters*, vol. 4, no. 2, pp. 1319–1326, 2019.

[20] Y. Umetani and K. Yoshida, "Continuous path control of space manipulators mounted on omv," *Acta Astronautica*, vol. 15, pp. 981–986, 1987.

[21] H. Mishra, M. De Stefano, A. M. Giordano, and C. Ott, "Output feedback stabilization of an orbital robot," in *2020 59th IEEE Conference on Decision and Control (CDC)*, 2020, pp. 1503–1501.

[22] A. Dietrich and C. Ott, "Hierarchical impedance-based tracking control of kinematically redundant robots," *IEEE Transactions on Robotics*, vol. 36, no. 1, pp. 204–221, 2020.

[23] S. Stramigioli, C. Secchi, A. van der Schaft, and C. Fantuzzi, "Sampled data systems passivity and discrete port-hamiltonian systems," *IEEE Transactions on Robotics*, vol. 21, no. 4, pp. 574–587, 2005.

[24] N. Kazantzis and C. Kravaris, "Time-discretization of nonlinear control systems via taylor methods," *Computers & Chemical Engineering*, vol. 23, no. 6, pp. 763–784, 1999.

[25] F. Caccavale, C. Natale, B. Siciliano, and L. Villani, "Six-dof impedance control based on angle/axis representations," *IEEE Transactions on Robotics and Automation*, vol. 15, no. 2, pp. 289–300, 1999.

[26] J. P. La Salle, *The Stability of Dynamical Systems*. Society for Industrial and Applied Mathematics, 1976.

[27] J. Grizzle and J.-M. Kang, "Discrete-time control design with positive semi-definite lyapunov functions," *Systems & Control Letters*, vol. 43, no. 4, pp. 287–292, 2001.

[28] M. A. Roa *et al.*, "Eross: In-orbit demonstration of european robotic orbital support services," in *2024 IEEE Aerospace Conference*, pp. 1–9.

[29] A. Albu-Schaffer *et al.*, "Cartesian impedance control of redundant robots: recent results with the dlr-light-weight-arms," in *IEEE International Conference on Robotics and Automation*, vol. 3, 2003, p. 3704.

[30] J. Artigas *et al.*, "The oos-sim: An on-ground simulation facility for on-orbit servicing robotic operations," in *IEEE International Conference on Robotics and Automation (ICRA)*, 2015, pp. 2854–2860.

[31] ——, "Teleoperation for on-orbit servicing missions through the astra geostationary satellite," in *IEEE Aerospace Conference*, 2016, pp. 1–12.